Combining attosecond XUV pulses with coincidence spectroscopy

M. Sabbar,[1,a),b)] S. Heuser,[1,a)] R. Boge,[1] M. Lucchini,[1] L. Gallmann,[1,2] C. Cirelli,[1] and U. Keller[1]
[1]*Department of Physics, ETH Zurich, 8093 Zurich, Switzerland*
[2]*Institute of Applied Physics, University of Bern, 3012 Bern, Switzerland*

(Received 25 July 2014; accepted 30 September 2014; published online 20 October 2014)

Here we present a successful combination of an attosecond beamline with a COLTRIMS apparatus, which we refer to as AttoCOLTRIMS. The setup provides either single attosecond pulses or attosecond pulse trains for extreme ultraviolet-infrared pump-probe experiments. We achieve full attosecond stability by using an active interferometer stabilization. The capability of the setup is demonstrated by means of two measurements, which lie at the heart of the COLTRIMS detector: firstly, we resolve the rotating electric field vector of an elliptically polarized few-cycle infrared laser field by attosecond streaking exploiting the access to the 3D momentum space of the charged particles. Secondly, we show streaking measurements on different atomic species obtained simultaneously in a single measurement making use of the advantage of measuring ions and electrons in coincidence. Both of these studies demonstrate the potential of the AttoCOLTRIMS for attosecond science. [http://dx.doi.org/10.1063/1.4898017]

I. INTRODUCTION

Today's attosecond pulse sources are based on the up-conversion of femtosecond lasers through the process of high harmonic generation (HHG).[1–3] Since the first confirmation of sub-femtosecond pulses in 2001,[4] the field of attosecond science has evolved rapidly. Shortly after the demonstration of attosecond pulse trains (APTs) strong evidence for the production of single attosecond pulses (SAPs) was observed.[5] This technological advance gave rise to further studies on electron dynamics occurring on its natural time-scale, which ranges from a few femtoseconds down to attoseconds.[6,7] Due to the lack of sufficient photon flux and low cross sections, experiments that have been carried out until today mostly rely on two-color pump-probe techniques using a combination of attosecond extreme ultraviolet and infrared (XUV and IR) pulses. Besides the traditional pump-probe approach there is also a more recently developed method with attosecond resolution available, which is known as the "Attoclock".[8,9] Being based on a short IR pulse alone this method was, e.g., used to extract the electron time delay in tunnel-ionization[9,10] as well as the timing in sequential double ionization of argon (Ar).[11]

One of the most crucial devices in attosecond science is the detector, which is eventually used to carry out the pump-probe experiment. There are mainly two types of detectors that are established today: spectrometers based on the measurement of photons and others that measure the momentum distribution of charged particles. Using XUV photon spectrometers pump-probe experiments can be conducted by attosecond transient absorption (ATA) spectroscopy.[6,12,13] In this method the absorption of the XUV spectrum in a dense target is recorded as a function of the XUV-IR delay. Charged particle spectrometers instead are based on the fact that XUV pulses or intense light fields can ionize atoms or molecules in single photon or multi-photon ionization, respectively. The detection of the charged fragments allows then to record the momentum distribution as a function of the pump-probe delay. The most common charged fragment detector is the time-of-flight (TOF) spectrometer.[14] Here, the particles are physically collected within a small solid angle, which effectively corresponds to the extraction of a 1D momentum distribution. More advanced spectrometers like the velocity-map imaging spectrometer (VMIS)[15] are able to resolve a 2D projection of the momentum distribution.

Direct access to the full 3D momentum distribution can be achieved with a COLTRIMS detector (COLd Target Recoil Ion Momentum Spectroscopy).[16,17] Here, the 3D momentum vector of each fragment is measured at the same time and for each fragmentation event. Moreover, it offers the unique possibility to assign an electron to its parent ion through momentum conservation, which is usually referred to as coincidence spectroscopy. This potentially allows addressing a broad range of open questions in attosecond science.

In this review article we describe, to our knowledge, the first successful combination of an ultra-stable attosecond interferometer with a COLTRIMS apparatus dubbed AttoCOLTRIMS. For a detailed description of a COLTRIMS device we refer the reader to the review articles in the references.[16,18] In Sec. II we present the description of the setup with particular emphasis on the design and performance of the actively stabilized interferometer. In Sec. III we show an example of a streaking experiment and the corresponding SAP characterization. In Sec. IV we demonstrate how the interplay of the angular resolution of the detector and the production of SAPs can be used to characterize the time-dependent electric field of the IR streaking field in 3D. In Sec. V we show how the coincidence capability of the detector

[a)]M. Sabbar and S. Heuser contributed equally to this work.
[b)]Electronic mail: msabbar@phys.ethz.ch

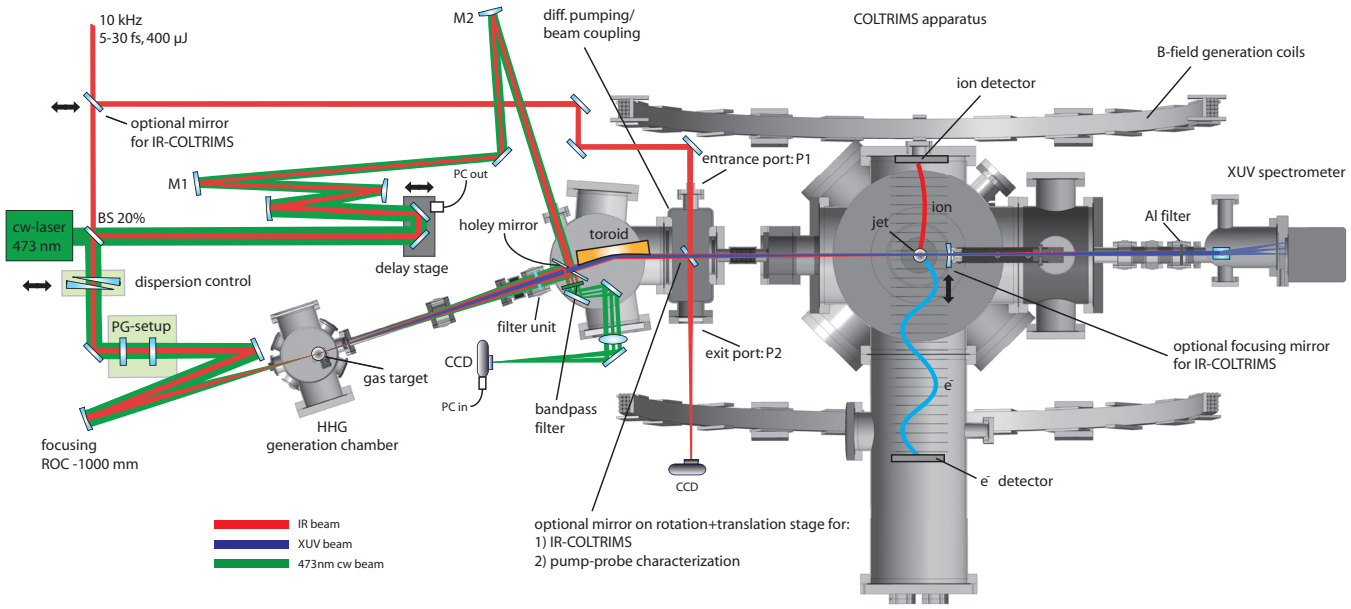

FIG. 1. Schematic representation of the combined attosecond beamline (left side) and COLTRIMS apparatus (right side). The IR driving pulses are divided into two parts by a 20% beam-splitter. The more intense portion is focused in the gas target in order to generate HH. The weaker part is sent through a delay line and then recombined with the XUV light by a holey mirror. Both beams are sent on a toroidal mirror, which has its focus in the interaction region of the COLTRIMS. The active stabilization system is depicted by the green line. A more detailed description can be found in the text.

can be used to simultaneously perform attosecond streaking measurements on different atomic species and how the dynamics in these systems can be compared under identical experimental conditions. Finally, in Sec. VI we provide a short summary and outlook.

II. EXPERIMENTAL SETUP

A. Overview

A schematic drawing of the AttoCOLTRIMS apparatus is shown in Fig. 1. The laser system used in our setup is a commercial carrier-envelope-phase (CEP) stabilized titanium-sapphire (Ti:sapph) amplifier (FEMTOPOWER compact V PRO CEP, Femtolasers). It provides pulse energies of 750 μJ with a pulse duration of 30 fs at a repetition rate of 10 kHz. These pulses are spectrally broadened in a Ne-filled hollow-core fiber[19] and subsequently compressed by chirped mirrors.[20] This results in few-cycle pulses of 5-6 fs with 400 μJ pulse energy and a spectral bandwidth that ranges from 550 to 950 nm at a central wavelength of about 770 nm.

The IR beam (red line in Fig. 1) passes a broadband beam-splitter, which has a reflectivity of 20%. The 80% portion, which is transmitted through the beam-splitter (pump) is used for HHG. For this purpose we focus the IR beam into an Ar filled gas target of 1 mm thickness using a spherical mirror with a radius of curvature of −1000 mm. The target itself is mounted in the vacuum chamber (labeled "HHG generation chamber" in Fig. 1). To precisely control its position the target is mounted on a manual xyz-translation-stage. The collinearly propagating high harmonic (HH) radiation and the generating IR beam are then exposed to a filter unit, which is described in detail in Sec. II C. The unit contains a drilled 1 mm thick fused silica plate, which has an outer diameter of 10 mm. The hole has a diameter of 3 mm and is covered by an aluminum (Al) foil of 300 nm thickness. The fused silica plate itself is mounted inside a vacuum valve allowing sealing the connection between the HHG chamber and the subsequent recombination/focusing chamber (filter unit is shown in the inset of Fig. 2). In this way, the purpose of the filter unit is twofold. On the one hand it serves as a high-pass filter for the HH radiation, blocking the IR. On the other hand it ensures that the vacuum pressure in the subsequent chambers is independent of the high pressure load in the HHG-chamber caused by the

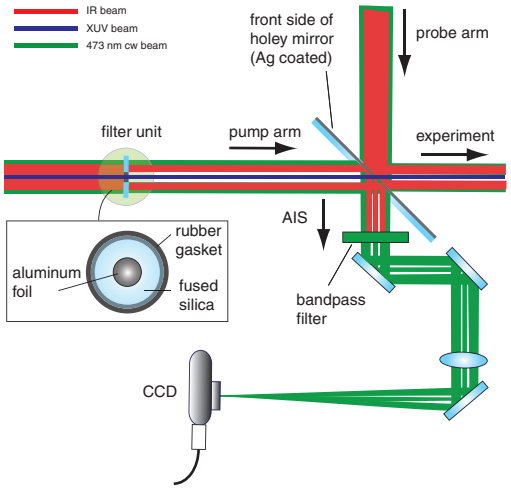

FIG. 2. Illustration of the beam paths for the AIS. The filter unit removes the central part of the IR beam and cw light in the pump arm. The remaining donut-shaped beam is reflected on the rear side of the holey mirror. Here it recombines with the light coming from the probe arm which passes through the hole of the mirror. After removal of the residual IR by the band-pass filter, the cw light is focused onto the CCD camera used to image the interference fringes. A more detailed description can be found in the text.

gas jet. After passing the Al foil the HH beam recombines with the previously split-off part of the IR (20%, probe) on a holey mirror with a central hole of 2.5 mm. Therefore, the beam path from the initial beam-splitter to this point forms a Mach-Zehnder type interferometer. To adjust the delay between the pump and probe arm we use a stack of two different translation stages. The first one is equipped with a DC motor with a long travel range allowing for a coarse adjustment of the temporal overlap. The second one is a piezo positioner (PZ 38 CAP, piezosystem Jena) used for the experiments. The piezo motion is controlled through a voltage between 0 and 10 V, where a voltage increment of 1 mV corresponds to 22.4 as in delay, leading to a full travel range of 224 fs. Finally, a toroidal mirror focuses both beams into the supersonic jet of the COLTRIMS detector creating charged fragments of the gas under investigation. The toroidal mirror is manufactured by the company Carl Zeiss AG. It is coated with an Au layer, which has a thickness of 30 nm, and has been designed with a focusing length of 800 mm. The reflectivity is about 70% for a wavelength of 800 nm, i.e., the IR-probe beam, and 65% for a wavelength of about 35 nm, i.e., the XUV-pump beam.

The gas jet is produced by supersonic expansion of a sample gas with a stagnation pressure at the back of the nozzle that can be varied between 1 and 10 bars. The direction of the supersonically expanded beam is vertical, from top to bottom; after the skimmer, which is 250 μm in diameter, the beam travels across a differential pumping stage and is dumped in a 10 mm hole. The distance between the skimmer and the interaction region, where the gas jet is about 1 mm thick, is 115 mm. Under typical conditions with 5 bar backing pressure of helium using a nozzle, which is 30 μm in diameter, the pressures in the jet source chamber and the beam dump are 1.4×10^{-4} mbar and 1.1×10^{-8} mbar, respectively. As a consequence, the estimated jet target density is in the range of 5×10^{10} atoms/cm^3. Under such conditions, usual ion and electron count rates are in order of 0.1 (0.2) ions (electrons) per laser shot. The background pressure in the main chamber is typically about 2.0×10^{-10} mbar without the presence of the target beam and about one order of magnitude higher with gas load, also depending on the target species.

After the interaction with the target jet, the XUV radiation reaches a spectrometer installed on the rear side of the COLTRIMS chamber. This allows for a fast and simultaneous acquisition of the high-harmonic spectrum. An additional Al foil of 500 nm thickness mounted on a mesh covers the entrance of the spectrometer in order to the residual IR radiation.

B. IR-only measurements

The COLTRIMS setup was previously used for IR-only experiments, e.g., in an "Attoclock" configuration using close-to-circular polarized IR pulses in combination with tight back-focusing. This focusing geometry thus allows achieving intensities up to several units of 10^{14} W/cm^2. At such intensities the ionization process in atoms is dominated by the tunneling process. Extensive studies on this topic have been carried out in our group using this detector.[8,9,21,22] To maintain the option to perform IR-only experiments, we incorporate the necessary details: the IR beam may alternatively be sent into vacuum via the entrance port P1 of the coupling chamber, where a movable mirror can be introduced in the beam path to reflect the light into the COLTRIMS chamber. The back-focusing mirror necessary for the IR-only experiments has been mounted on a manipulator placed in the COLTRIMS chamber, which allows for precise alignment of its position as well as complete removal while XUV-IR experiments are performed.

C. Actively stabilized interferometer

Attosecond interferometric stability of the pump-probe setup is a technical challenge. For instance, changing the optical path length of one arm of the interferometer by 30 nm with respect to the other already introduces a temporal delay of 100 as. There are two established approaches in order to achieve such a stability: passively stable setups where all mechanical components of the interferometer are chosen carefully and placed on a single temperature-stabilized optical table within a vacuum chamber[23] or actively stabilized setups in which the length of one arm of the interferometer is actively adjusted with respect to the other by using a frequency-stable reference laser.[24] While it has been demonstrated that passively stable setups can provide a short-term stability of well below 100 as, long-term stability and repeatability cannot be guaranteed. Since a COLTRIMS apparatus needs to be operated at a count rate, which is significantly lower than the laser repetition rate in order to avoid potential false coincidences, generally measurements can take much longer compared to other detectors. Therefore, the use of an actively stabilized interferometer is highly desirable for reliable pump-probe measurements.

We have implemented such an active interferometer stabilization (AIS) allowing the use of few-cycle pulses at 10 kHz repetition rate adapting some of the ideas mentioned by Chini *et al.*[24] We use a continuous wave (cw) laser with a wavelength of 473 nm (Cobolt Blues, Cobolt AB) coupled into the interferometer via the 20% beam-splitter (green beam path in Fig. 1). Both split parts of the beam are exposed to the same optics as the IR and finally recombine on the rear side of the holey mirror. The Al filter unit is designed to allow part of the cw-laser to reach the rear side of the holey mirror and at the same time to prevent the generating IR beam from passing. As can be seen from the inset of Fig. 2, we use an Al foil mounted on a drilled fused silica ring. The donut-shaped cw- and IR beams are then reflected on the rear side of the holey mirror (see Fig. 2). Since the holey mirror has a substrate thickness of only 1 mm a substantial fraction of the cw beam in the probe arm passes through the hole. A bandpass filter at 470 nm with a bandwidth of 10 nm is then used to filter out the residual IR beam. In order to detect the interference pattern, the cw beams are subsequently imaged onto a charged-coupled device (CCD) camera. A home-built software stabilizes the spatial interference fringes by a feedback voltage to the piezo translation stage of the delay unit. With this approach we exclude any long-term drift and we can compensate for a potential hysteresis of the piezo. The AIS has been also characterized quantitatively as can be seen in Fig. 3. For this purpose we have recorded the

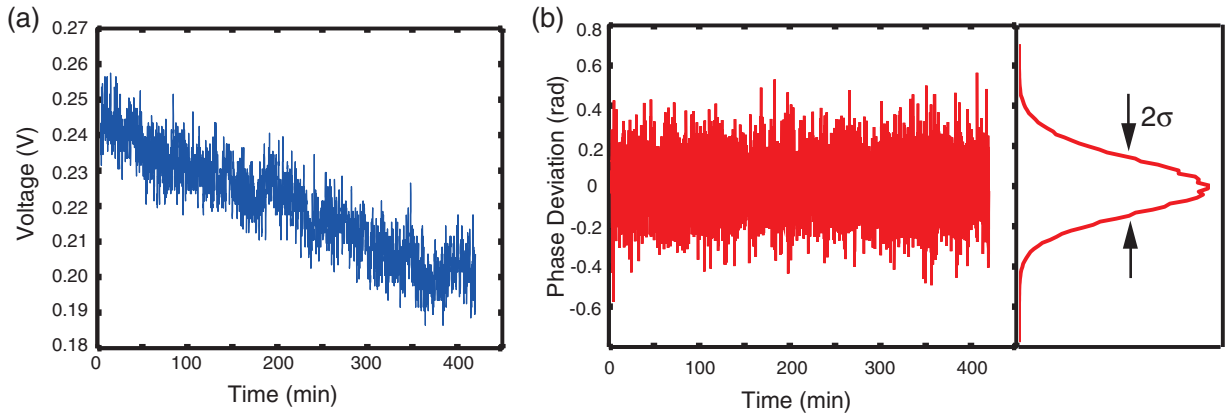

FIG. 3. Characterization of the AIS. (a) Evolution of the control voltage applied to the piezo translation stage while operating the AIS over 7 h. (b) Variation of the recorded phase over the same time interval yielding a standard deviation of about 60 as.

root-mean-square (RMS) deviation of the phase over approximately 7 h. The analysis reveals that the standard deviation (one σ) is smaller than 60 as.

It is worth emphasizing that the implementation of our AIS is different from others reported so far. First of all we use a blue cw-laser at 473 nm instead of a helium-neon laser or a frequency-doubled green laser. The reason is the following: provided that the reference laser is co-propagating with the IR it needs to be ensured that the IR can be filtered out. This allows imaging the interference pattern of the cw beam onto the CCD camera without a superimposed IR. The filtering can be achieved with a chopper which mechanically blocks the IR pulses at its repetition rate. Since choppers at 10 kHz produce significant vibrations we decided to use a cw-laser at a frequency that does not overlap with the spectral region of the output of our hollow-core fiber compression setup. The use of a bandpass filter for the cw, therefore, allows blocking the IR pulses. Another important difference is that we have used a holey mirror with a thin substrate and a silver coating instead of a dielectric mirror as reported in reference.[24] This allows us to employ broadband, few-cycle laser pulses since the reflectivity of dielectric mirrors is limited to relatively small spectral bandwidths.

III. XUV-IR PUMP-PROBE EXPERIMENTS AND XUV PULSE CHARACTERIZATION

In this section, we present an example of a streaking measurement for SAP characterization. We generate APTs by focusing the linearly polarized IR beam into an Ar gas jet. For the generation of SAPs we employ a polarization gate[25] (PG) before generating the HH. By manipulating the polarization of the IR field with the help of a quartz plate and a broadband quarter-wave plate it is possible to confine the HHG to one half-cycle of the IR field and thereby to select only one SAP. For the pump-probe alignment we use the same optional mirror in the coupling chamber that also allows for the IR-only experiments described in Sec. II A (see Fig. 1). Turning it by 180° and removing the filter unit allows coupling the IR pump and probe beams out via the exit port P2. Both beams are subsequently imaged onto a CCD camera. The temporal overlap of the pulses from both arms is adjusted through the delay stage by monitoring the appearance of spectral fringes. The spatial overlap is achieved by the alignment of two motorized mirrors in the probe arm labeled as M1 and M2.

APTs and SAPs can be temporally characterized by two different measurement techniques, namely, the RABBITT (Reconstruction of Attosecond Beating By Interference of Two-photon Transitions)[26] and the attosecond streaking technique.[27] Both of them are experimentally similar, but their theoretical description relies on different approaches corresponding to different intensity regimes of the IR. In both methods, the collinearly propagating XUV and IR pulses (overlapping both in time and space) are focused into the supersonic gas jet, containing, e.g., noble gas atoms, inside the COLTRIMS chamber. The gas is ionized by single photon excitations by the part of the XUV photon energies that lies above the ionization threshold. Thus, an (truncated) electron replica of the photon spectrum is generated. In the case of streaking, when pump and probe beams overlap in time, the IR beam, not intense enough to ionize the atoms, acts as an ultrafast phase modulator on the electron spectrum. Recording the modulated spectra as a function of the XUV-IR delay delivers a spectrogram (see Fig. 4), which can be used to extract the temporal properties of the XUV pulse(s). The IR energetically shifts the continuous electron spectrum by a value that is proportional to its vector potential at the instant of ionization. This effect can be explained in a classical picture, where the electrons experience a force given by the electric field of the laser. In the case of RABBITT, when pump and probe are not overlapping, the electron spectrum is characterized by discrete peaks at the harmonics positions. For small values of the XUV-IR delay, an oscillatory signal, so called sidebands (SB), appears between the main peaks. The SB signal results from the interference of two different excitation pathways involving the absorption of one HH photon and absorption or emission of one IR photon. Since two indistinguishable pathways lead to the same final state of each SB, the SB signal will oscillate as a function of the XUV-IR delay with a frequency that is given by twice the IR carrier frequency. The group delay of the HH is encoded in the phase of the SB signal.

In the following, we present the temporal properties of the SAPs. Figure 4(a) shows an attosecond streaking spectrogram, measured in Ne with a data acquisition time of

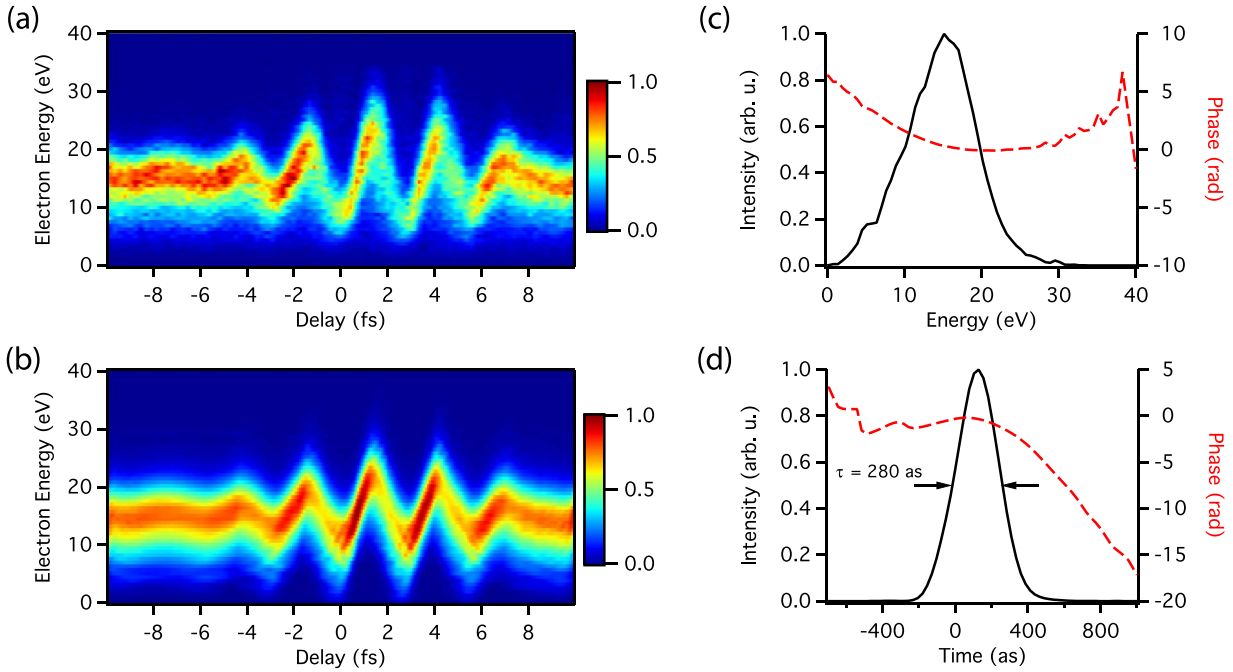

FIG. 4. Reconstruction of a SAP produced with our setup. (a) Attosecond streaking spectrogram measured with the COLTRIMS apparatus using Ar for the HHG and neon (Ne) as the target gas. This high-quality streaking trace was acquired in about 90 min. (b) FROG-CRAB reconstruction of the trace. (c) Reconstructed spectrum and phase of the pulse corresponding to a GDD of 16000 as^2 (d) The time-domain representation reveals a pulse duration of 280 as.

about 90 min. Among the few existing reconstruction algorithms, we chose the most established one called Frequency-Resolved Optical Gating for Complete Reconstruction of Attosecond Bursts (FROG-CRAB).[28] Similar to the classical FROG method[29] used for visible and IR pulses it is based on an iterative routine that generates a 2D streaking spectrogram, which converges to the measured data taking into account the constraints of the measurement process. One of the resulting quantities is the pulse's phase. As shown in Fig. 4(d) the pulse has a duration of 280 as. The reconstruction also reveals that the pulses suffer from overcompensated chirp of about 16000 as^2. Using a thinner Al foil in the XUV beam path would allow to compress the pulses closer to their transform-limit, which is about 165 as.[30]

IV. RESOLVING THE TIME-DEPENDENT ELECTRIC FIELD VECTOR IN 3D

In this section, we will present how the combination of attosecond streaking and a COLTRIMS detector naturally allows extracting the electric field of the IR streaking light in 3D. As mentioned above, in conventional attosecond streaking experiments the electrons are detected in a TOF detector. These detectors are equipped with a skimmer in front of the MCP in order to collect electrons only within a small angle and thereby avoiding any ambiguities of the electron energies. In this configuration it is always preferential to choose both the XUV and the streaking field polarization parallel to the skimmer-MCP axis. This ensures best collection efficiency and highest energy streaking amplitudes. In the limiting case, where the streaking polarization is perpendicular to the aforementioned axis there will not be any measurable streaking effect. In a COLTRIMS apparatus the electron momenta are measured within the full solid angle. The latter allows streaking to be measured equally in every direction, thus enabling the full 3D characterization of the IR field. To demonstrate this potential we have performed an attosecond streaking experiment with an elliptically polarized IR streaking field using Ar as a target gas. To produce elliptical polarization at the position of the COLTRIMS target we have used a combination of a λ/2- and λ/4-plate placed right before the holey mirror. The λ/2-wave plate allows to partly compensate for the effects on the IR polarization of the optics following the holey and toroidal mirrors. For a fast characterization of the degree of ellipticity, we made use of a multi-photon effect known as above-threshold ionization (ATI). In this process atoms are ionized by the simultaneous absorption of several photons thereby generating electrons and ions, which are detectable with the COLTRIMS apparatus. This effect scales nonlinearly with the peak intensity of the IR pulses, providing a rough characterization of the ellipticity. Starting from linear polarization the signal then needs to be minimized with the help of the wave plates to obtain the highest degree of ellipticity.

Using the above-mentioned procedure to obtain elliptically polarized IR pulses we have then performed an attosecond streaking measurement to retrieve the vector potential of the IR. Here, the liberated electrons are accelerated by the force $\mathbf{F}_{\mathrm{el}} = -e\mathbf{E}_{\mathrm{IR}}(t)$ according to the electric field of the IR $\mathbf{E}_{\mathrm{IR}}(t)$ at the instance of ionization. Hence, depending on their time of birth t_0 the final electron momenta are given by

$$\mathbf{p}(t_0) = \mathbf{p}_0 - \frac{e}{m}\int_{t_0}^{\infty} \mathbf{E}_{\mathrm{IR}}(t)dt = \mathbf{p}_0 - \frac{e}{m}\mathbf{A}_{\mathrm{L}}(t_0),$$

where e is the electron charge, m is the electron mass, $\mathbf{p}_0$ is the initial momentum of the electron, and $\mathbf{A}_{\mathrm{L}}(t_0) = \int_{t_0}^{\infty} \mathbf{E}_{\mathrm{IR}}dt$

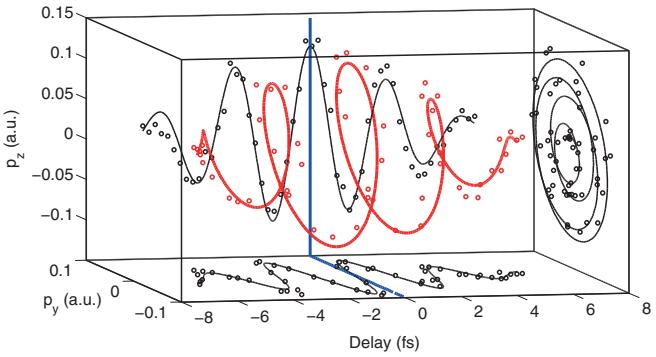

FIG. 5. 3D reconstruction of the vector potential of an elliptically polarized few-cycle IR pulse by attosecond streaking in the COLTRIMS apparatus. The red circles/line show the motion of the center-of-mass (COM) of the electron distribution modulated by the IR pulse. The projections of the oscillation are presented in black. The expected phase shift of about 90° between the *y*- and *z*-component of the light field can already be seen from the blue lines drawn at a delay position of 0 fs.

is the vector potential at the moment of birth of the electron. Performing a center-of-mass (COM) analysis on the streaking traces along each momentum component of the electron spectra, therefore, allows identifying $(e/m)\mathbf{A}_L(t)$ approximately as the oscillation around the central momentum $\mathbf{p}_0$.

Figure 5 shows the *y*- and *z*-components (IR polarization plane) of the electron momentum distribution as a function of the SAP-IR delay. Both components are retrieved by a COM analysis in each of the two projections of the streaking trace, which in this case has been recorded within 20 min. A phase shift close to 90° between the two traces already indicates the elliptical nature of the polarization. Quantitatively, we have extracted an ellipticity of $\varepsilon = 0.69$ and an angle $\beta = 104.5°$ of the ellipse's major axis relative to the p_y-axis by fitting an analytic expression to the data. This method can easily be extended to more complex electric field configuration with time-dependent polarization states, as there are no constrains to the IR pulse shape.

V. USING COINCIDENCE SPECTROSCOPY TO ACCESS DELAYS IN PHOTOEMISSION

Photoemission is one of the most fundamental processes in physics and occurs on a timescale of attoseconds. With today's advanced light sources approaching the atomic unit of time (24 as) time-resolved photoemission is no longer only a domain of theoretical research. Pioneering work on this topic was carried out by Schultze *et al.*[7] Using the attosecond streaking technique with sufficiently high photon energies Schultze and co-workers measured the photoemission time delay between the 2*s*- and 2*p*-electrons in Ne to be about 21 as. Shortly afterwards Klünder *et al.*[31] applied the RABBITT technique to measure the delay between the 3*s*- and 3*p*-electrons in Ar presenting an energy-dependent time delay.

In both of these exciting experiments an important requirement for the data analysis was to have the spectrograms of the two initial states well separated in energy. This allows to spectrally distinguish electrons emitted either from the *s*- or *p*-state. Therefore, if the energetic separation of the two states would be smaller than the spectral bandwidth of the attosecond pulses, a delay extraction would have been impossible. It follows that this method fails to disclose photoemission delays between electrons originating from initial states, which are too close in energy, e.g., two electronic states of different noble gases. Taking advantage of the coincidence detection, we are able to overcome this problem and resolve relative photoemission delays of species with similar ionization potentials. Figure 6 presents a measurement in which the coincidence capability is needed. Using a gas mixture (50% Ar and 50% Ne in this case) it is possible to directly assign electrons to their parent ions, while both species are exposed to identical laser conditions. Therefore, it is straightforward to extract multiple spectrograms (Fig. 6(b) upper and lower panels) from a single measurement (Fig. 6(a)). Using the FROG-CRAB analysis on the disentangled traces allows extracting the delay in photoionization between Ar and Ne thus revealing the benefit of a COLTRIMS apparatus for attosecond science.

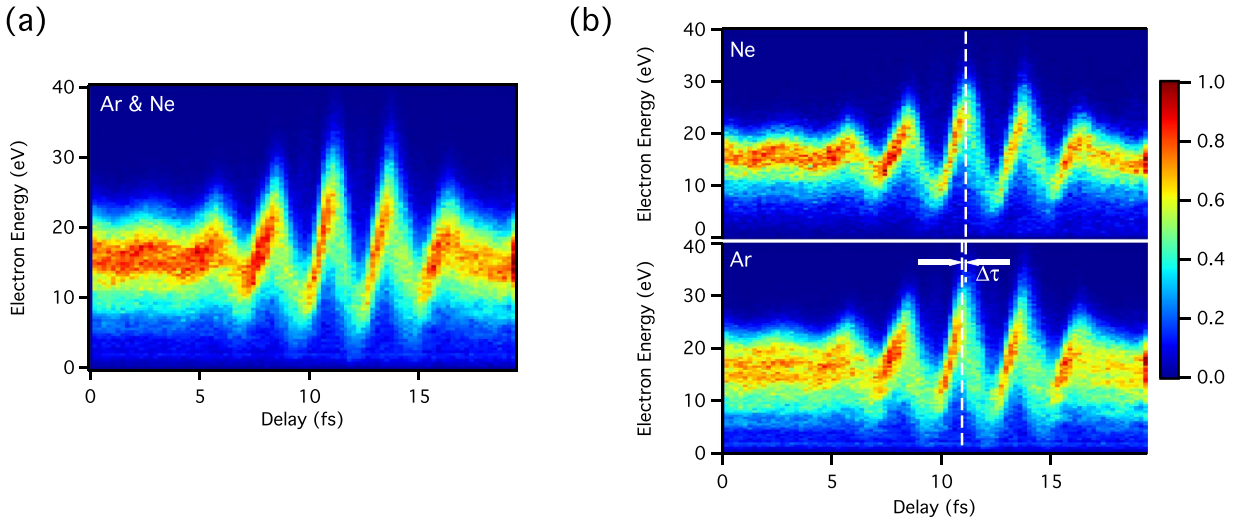

FIG. 6. Simultaneous attosecond streaking of electrons originating from Ar and Ne. (a) A streaking spectrogram is measured containing electron of both species. (b) Using the coincidence capability of the COLTRIMS detector the electrons from either species are disentangled from the trace in (a), thus giving the possibility to measure photoemission delays even though the electron energies overlap.

The physics that can be extracted from these measurements is discussed in detail in Ref. 32.

VI. SUMMARY

In conclusion, we have presented a combination of an attosecond interferometric beamline with a COLTRIMS apparatus, which we refer to as AttoCOLTRIMS. We have described its versatile design, which allows for easy switching between strong-field IR studies and XUV-IR pump-probe experiments. We implemented and fully characterized an active stabilization of our interferometer revealing long-term stability over more than 7 h with a standard deviation smaller than 60 as. This makes the stabilization scheme extremely suitable for experiments in which long data acquisition and attosecond resolution are required at the same time. Taking advantage of this feature, we presented first streaking measurements with a COLTRIMS detector and demonstrate that our apparatus can be employed to fully characterize SAPs using the FROG-CRAB technique. Furthermore, having access to the 3D momentum vector of each particle, we demonstrated for the first time the possibility to fully resolve the time-dependent electric field vector of elliptically polarized light in 3D. In a second measurement we showed how the coincidence capability of the COLTRIMS apparatus can be used to extract photoionization time delays between different atomic species with similar ionization potentials. Besides ongoing work on atomic and molecular photoemission time delays, angle-resolved experiments are currently being carried out. Future work will also include other unique possibilities of the COLTRIMS detector such as the access to the molecular frame.

ACKNOWLEDGMENTS

This work was supported by the ERC advanced Grant No. ERC-2012-ADG_20120216 within the seventh framework program of the European Union and by the NCCR MUST, funded by the Swiss National Science Foundation. M.L. acknowledges support from the ETH Zurich Postdoctoral Fellowship Program.

[1]A. McPherson, G. Gibson, H. Jara, U. Johann, T. S. Luk, I. A. McIntyre, K. Boyer, and C. K. Rhodes, J. Opt. Soc. Am. B **4**, 595 (1987).
[2]M. Ferray, A. L'Huillier, X. F. Li, L. A. Lompré, G. Mainfray, and C. Manus, J. Phys. B **21**, L31 (1988).
[3]P. Antoine, A. L'Huillier, and M. Lewenstein, Phys. Rev. Lett. **77**, 1234 (1996).
[4]P. M. Paul, E. S. Toma, P. Breger, G. Mullot, F. Augé, P. Balcou, H. G. Muller, and P. Agostini, Science **292**, 1689 (2001).
[5]R. K. M. Hentschel, Ch. Spielmann, G. A. Reider, N. Milosevic, T. Brabec, P. Corkum, U. Heinzmann, M. Drescher, and F. Krausz, Nature (London) **414**, 509 (2001).
[6]E. Goulielmakis, Z. H. Loh, A. Wirth, R. Santra, N. Rohringer, V. S. Yakovlev, S. Zherebtsov, T. Pfeifer, A. M. Azzeer, M. F. Kling, S. R. Leone, and F. Krausz, Nature (London) **466**, 739 (2010).
[7]M. Schultze, M. Fiess, N. Karpowicz, J. Gagnon, M. Korbman, M. Hofstetter, S. Neppl, A. L. Cavalieri, Y. Komninos, T. Mercouris, C. A. Nicolaides, R. Pazourek, S. Nagele, J. Feist, J. Burgdorfer, A. M. Azzeer, R. Ernstorfer, R. Kienberger, U. Kleineberg, E. Goulielmakis, F. Krausz, and V. S. Yakovlev, Science **328**, 1658 (2010).
[8]P. Eckle, M. Smolarski, P. Schlup, J. Biegert, A. Staudte, M. Schöffler, H. G. Muller, R. Dörner, and U. Keller, Nature Phys. **4**, 565 (2008).
[9]P. Eckle, A. N. Pfeiffer, C. Cirelli, A. Staudte, R. Dörner, H. G. Muller, M. Büttiker, and U. Keller, Science **322**, 1525 (2008).
[10]A. S. Landsman, M. Weger, J. Maurer, R. Boge, A. Ludwig, S. Heuser, C. Cirelli, L. Gallmann, and U. Keller, e-print arXiv:1301.2766v2.
[11]A. N. Pfeiffer, C. Cirelli, M. Smolarski, R. Dorner, and U. Keller, Nature Phys. **7**, 428 (2011).
[12]H. Wang, M. Chini, S. Chen, C.-H. Zhang, F. He, Y. Cheng, Y. Wu, U. Thumm, and Z. Chang, Phys. Rev. Lett. **105**, 143002 (2010).
[13]M. Holler, F. Schapper, L. Gallmann, and U. Keller, Phys. Rev. Lett. **106**, 123601 (2011).
[14]O. Hemmers, S. B. Whitfield, P. Glans, H. Wang, D. W. Lindle, R. Wehlitz, and I. A. Sellin, Rev. Sci. Instrum. **69**, 3809 (1998).
[15]A. T. J. B. Eppink and D. H. Parker, Rev. Sci. Instrum. **68**, 3477 (1997).
[16]R. Dörner, V. Mergel, O. Jagutzki, L. Spielberger, J. Ullrich, R. Moshammer, and H. Schmidt-Bocking, Phys. Rep. **330**, 95 (2000).
[17]J. Ullrich, R. Mooshammer, A. Dorn, R. Dörner, L. P. H. Schmidt, and H. Schmidt-Böcking, Rep. Prog. Phys. **66**, 1463 (2003).
[18]J. Ullrich, R. Moshammer, R. Dörner, O. Jagutzki, V. Mergel, H. Schmidt-Böcking, and L. Spielberger, J. Phys. B **30**, 2917 (1997).
[19]M. Nisoli, S. De Silvestri, O. Svelto, R. Szipöcs, K. Ferenz, C. Spielmann, S. Sartania, and F. Krausz, Opt. Lett. **22**, 522 (1997).
[20]F. X. Kärtner, U. Morgner, R. Ell, T. Schibli, J. G. Fujimoto, E. P. Ippen, V. Scheuer, G. Angelow, and T. Tschudi, J. Opt. Soc. Am. B **18**, 882 (2001).
[21]A. N. Pfeiffer, C. Cirelli, M. Smolarski, D. Dimitrovski, M. Abu-samha, L. B. Madsen, and U. Keller, Nature Phys. **8**, 76 (2012).
[22]R. Boge, C. Cirelli, A. S. Landsman, S. Heuser, A. Ludwig, J. Maurer, M. Weger, L. Gallmann, and U. Keller, Phys. Rev. Lett. **111**, 103003 (2013).
[23]R. Locher, M. Lucchini, J. Herrmann, M. Sabbar, M. Weger, A. Ludwig, L. Castiglioni, M. Greif, M. Hengsberger, L. Gallmann, and U. Keller, Rev. Sci. Instrum. **85**, 013113 (2014).
[24]H. M. M. Chini, H. Wang, S. Chen, C. Yun, S. Scott, S. Gilbertson, and Z. Chang, Opt. Exp. **17**, 21459 (2009).
[25]I. J. Sola, E. Mével, L. Elouga, E. Constant, V. Strelkov, L. Poletto, P. Villoresi, E. Benedetti, J.-P. Caumes, S. Stagira, C. Vozzi, G. Sansone, and M. Nisoli, Nature Phys. **2**, 319 (2006).
[26]Y. Mairesse, A. de Bohan, L. J. Frasinski, H. Merdji, L. C. Dinu, P. Monchicourt, P. Breger, M. Kovačev, R. Taïeb, B. Carré, H. G. Muller, P. Agostini, and P. Salières, Science **302**, 1540 (2003).
[27]J. Itatani, F. Quéré, G. L. Yudin, M. Y. Ivanov, F. Krausz, and P. B. Corkum, Phys. Rev. Lett. **88**, 173903 (2002).
[28]Y. Mairesse and F. Quéré, Phys. Rev. A **71**, 011401(R) (2005).
[29]K. W. DeLong, D. N. Fittinghoff, R. Trebino, B. Kohler, and K. Wilson, Opt. Lett. **19**, 2152 (1994).
[30]R. Lopez-Martens, K. Varju, P. Johnsson, J. Mauritsson, Y. Mairesse, P. Salieres, M. B. Gaarde, K. J. Schafer, A. Persson, S. Svanberg, C.-G. Wahlstrom, and A. L'Huillier, Phys. Rev. Lett. **94**, 033001 (2005).
[31]K. Klünder, J. M. Dahlström, M. Gisselbrecht, T. Fordell, M. Swoboda, D. Guenot, P. Johnsson, J. Caillat, J. Mauritsson, A. Maquet, R. Taïeb, and A. L'Huillier, Phys. Rev. Lett. **106**, 143002 (2011).
[32]M. Sabbar, S. Heuser, R. Boge, M. Lucchini, L. Gallmann, C. Cirelli, and U. Keller, e-print arXiv:1407.6623.